IEEE Access
Multidisciplinary ⋮ Rapid Review ⋮ Open Access Journal

Received 25 September 2023, accepted 9 October 2023, date of publication 11 October 2023, date of current version 18 October 2023.

Digital Object Identifier 10.1109/ACCESS.2023.3323933

RESEARCH ARTICLE

A Novel Double Stator Hybrid-Excited Flux Reversal Permanent Magnet Machine With Halbach Arrays for Electric Vehicle Traction Applications

SHICHAO NING[1,2], PATTASAD SEANGWONG[1], NUWANTHA FERNANDO[3], (Member, IEEE), JONGGRIST JONGUDOMKARN[1], APIRAT SIRITARATIWAT[1], AND PIRAT KHUNKITTI[1], (Member, IEEE)

[1]Department of Electrical Engineering, Faculty of Engineering, Khon Kaen University, Khon Kaen 40002, Thailand
[2]College of Information, Mechanical and Electrical Engineering, Ningde Normal University, Ningde 352100, China
[3]School of Engineering, Royal Melbourne Institute of Technology (RMIT), Melbourne, VIC 3000, Australia

Corresponding author: Pirat Khunkitti (piratkh@kku.ac.th)

This work was supported in part by the National Research Council of Thailand and Khon Kaen University under Grant N42A660360, in part by the Major Science and Technology Innovation Projects in Fujian Province under Grant 2021G02016, in part by the Natural Science Foundation of Fujian Province under Grant 2023J01352, in part by the Joint Enterprise Research Project under Grant 2022ZX305, and in part by the Youth Fund Project of Ningde Normal University under Grant 2019Q106.

ABSTRACT This research paper introduces a novel double-stator (DS) hybrid-excited (HE) flux reversal permanent magnet (FRPM) machine with Halbach PM arrays, specifically designed for electric vehicle (EV) traction applications. The study commences with a detailed description of the operating principle of the proposed machine. The machine design incorporates a comprehensive sensitivity analysis of its structural design variables, followed by a multi-objective optimization utilizing the NSGA-II algorithm. The results clearly show that the proposed DS-HE-FRPM machine outperforms the benchmark in several key aspects while adhering to the same PM volume constraint. It exhibits significantly improved back electromotive force, and substantially lower cogging torque. Notably, when compared to the benchmark, the optimized structure of the DS-HE-FRPM machine highlights a notable 22.4% enhancement in electromagnetic torque, while effectively keeping torque ripple at a low level. The underlying reasons behind these notable improvements of the proposed machine structure are explained in detail, providing a comprehensive understanding of their rationales. These findings suggest that the innovative DS-HE-FRPM machine holds significant torque potential, which could greatly enhance the performance and efficiency of EVs. This represents a highly promising development in the field of traction applications.

INDEX TERMS Permanent magnet machine, flux reversal, Double stator, Halbach permanent magnet array, hybrid excitation.

I. INTRODUCTION

Flux reversal permanent magnet (FRPM) machines are highly promising for a wide range of applications, such as electric vehicles (EVs), aerospace, low-speed servo, and wind power generation, owing to their simple structure, robust unexcited reluctance rotor, high winding utilization, and wide-range operation [1], [2], [3]. However, the dual salient pole structure of FRPM machines, with permanent magnets (PMs) mounted on the stator teeth surface, leads to several drawbacks. These include high torque ripple and cogging torque, limited flux regulation capability due to the fixed air-gap flux of PMs, relatively high flux leakage, and lower torque density compared to other stator-PM machines [4], [5], [6]. Various

The associate editor coordinating the review of this manuscript and approving it for publication was Xiaodong Liang.

approaches have been proposed in the literature to address the limitations of FRPM machines. These include modifications to the structural configuration, winding configuration, PM arrangement, as well as the utilization of advanced design techniques such as transverse-flux configurations, partitioned stator (PS), double-stator (DS), hybrid excitation (HE) and Halbach magnet arrays [7], [8], [9], [10]. Among these approaches, the latter three approaches have been thoroughly studied and well-documented in the literature to enhance the performance of PM machines specifically for applications that demand high torque requirements.

The HE technique features DC excitation along with armature excitation. This technique has been extensively studied in the literature to extend the operating range, improve torque density, and enhance the flux regulation capability of several PM machines. In [6], a HE technique was proposed and implemented to enhance the electromagnetic performance and flux regulation capability of the PS-HE-FRPM machine. In 2019, a comprehensive review of HE machine topologies was conducted [7]. The study concludes that the HE technique can effectively regulate the magnetic field, leading to enhanced low-speed torque and a wider operating range. Z. Pan et al. proposed a stator-FRPM machine with an arc PM configuration. It was demonstrated that this design offers higher torque density, lower torque ripple, and a wider range of flux regulation capability compared to traditional designs [8]. Additionally, an investigation on asymmetric consequent-pole HE-FRPM machines, exploring two different asymmetrical topologies was conducted by Wei et al. [9]. This study reveals a novel understanding of the relationship between torque components generated by airgap magnetic field space harmonics and the phase shift between the phase flux-linkages due to the DC excitation and the PM fixed excitation.

In addition, reducing magnetic flux leakage within the structure of the PM machine is an essential aspect of enhancing the performance of FRPM machines. One effective approach to achieve this is through the utilization of Halbach PM arrays. These arrays consist of PMs with different polarities combined in a specific configuration. They not only minimize flux leakage throughout the PM machine's structure but also mitigate the risk of demagnetization. The use of Halbach PM arrays has been widely used to improve the performance of PM machines. In 2009, the Halbach PM arrangements were installed on a surface-mounted PM machine, which led to a potential reduction in flux leakage and demagnetization risk [10]. Similarly, Shen et al. demonstrated the effectiveness of Halbach PM arrays by filling the slot opening of a vernier reluctance linear machine with a Halbach arrangement, leading to a significant improvement of over 30% in thrust force density [11]. Additionally, Du et al. introduced a PS-HE machine with slot Halbach permanent magnet arrays, which exhibited a remarkable 76% increase in torque output compared to the conventional PS-HE machine, while simultaneously reducing the occurrence of PM flux leakage within stator [12]. Recently, a consequent-pole FRPM machine structure integrated with Halbach arrays was proposed [5]. This configuration not only enhances torque output but also reduces flux leakage without compromising efficiency.

In recent years, double-stator PM machines have garnered attention due to their potential high performance. The incorporation of a double-stator configuration in PM machines has shown promising results in terms of torque density, power factor, and efficiency improvements. In 2014, a DS vernier PM machine was investigated, showcasing a higher power factor and increased torque capacity, especially at low speeds [13]. Another noteworthy development exhibiting superior electromagnetic performance, higher flux regulation capability, and a lower cost for a DS-HE flux-switching machine utilizing ferrite magnets for excitation was presented in [14]. Gao et al. demonstrate the application of the DS technique, focusing on a vernier PM machines with a consequent-pole Halbach-array PM rotor offering higher torque density, improved efficiency, and lower cogging torque compared to the conventional designs [15].

Literature on FRPM machines also identifies several weak points such as weak flux regulation capability, relatively large flux leakage, and high torque ripple and cogging torque. To address these limitations, this paper introduces a novel double-stator hybrid excited flux reversal permanent magnet (DS-HE-FRPM) machine with Halbach PM arrays. To-date combination of these techniques has not been applied to FRPM machine design and is one of the key contributions presented in this paper. The machine design was carried out through a sensitivity analysis of key design variables, followed by a multi-objective optimization using the NSGA-II algorithm, based on finite element analysis. The primary objective of the design was chosen to enhance torque density, suppress torque ripple, reduce flux leakage, and ultimately achieve superior overall performance.

The manuscript is arranged as follows: Section II explains the topology and operating principles of the DS-HE-FRPM machine, while Section III outlines the optimization of the design using the NSGA-II algorithm. Section IV evaluates the electromagnetic performance of the proposed machine using 2-D finite element analysis and compares it with a benchmark FRPM machine. Finally, conclusions are drawn in Section V.

II. MACHINE TOPOLOGY AND OPERATING PRINCIPLE

Fig. 1(a) presents the benchmark three-phase FRPM machine adopted from [1]. This design has been extensively studied for its exceptional low-speed/high torque operation, overload capability, high torque density and flux-weakening capabilities. This machine features a 12-stator slot/17-rotor pole HE structure, where both the armature and DC field windings are placed within the same stator slot. Each stator tooth contains two PMs of the same polarity, while the adjacent teeth have PMs with opposite polarity. To enhance its performance, a novel design referred to as the DS-HE-FRPM machine is proposed in this paper and depicted in Fig. 1(b). The main specifications of this design are provided in Table 1.

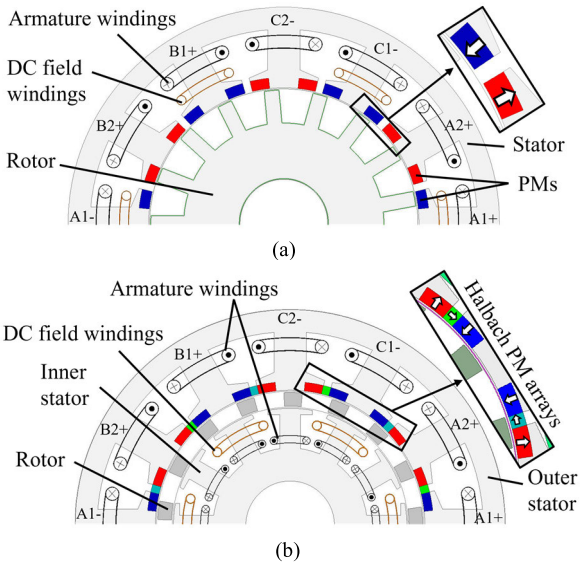

FIGURE 1. Topology of (a) the benchmark and (b) the DS-HE-FRPM machine.

TABLE 1. Main specification of machines.

Items (unit)	Benchmark FRPM	DS-HE-FRPM
Stator slots number, N_s	12	
Rotor pieces number, N_r	17	
Rated speed (r/min)	300	
Air-gap length (mm)	0.65	
Stack length (mm)	75	
Outer stator radius (mm)	63	
Stator inner radius (mm)	39.5	
Stator slot opening ratio	0.1	
Rotor slot opening ratio	0.7	-
Inner stator outer radius (mm)	-	34.2
Inner stator inner radius (mm)	-	13
Outer stator tooth width (mm)	9.45	
PM pole arc (degree)	7.45	
PM material	N40SH	
PM volume (mm^3)	28800	
Field winding turns	76	
Ratio of field winding to total winding	1/3	-
Outer armature winding turns	38	58
Inner armature winding turns	-	14
AC current density (A/mm^2)	2.3	

The DS-HE-FRPM configuration incorporates a double-stator arrangement with hollow rotor constructed in the form of iron pole pieces sandwiched between the two stators. The inner and outer stator teeth are in alignment and aims to enhance the machine's flux regulation capability. The number of inner stator and outer stator teeth, as well as the rotor pole, remains consistent with benchmark design. The determination of the appropriate number of stator teeth and rotor poles can be achieved by employing a theoretical expression specifically developed for initializing the number of pole combinations of FRPM machines, denoted as (1) [16]:

$$P_r = 3P_s \pm K \tag{1}$$

where P_s, P_r, and K are the number of stator slots, the number of rotor pole pieces, and the stator pole-pairs, respectively.

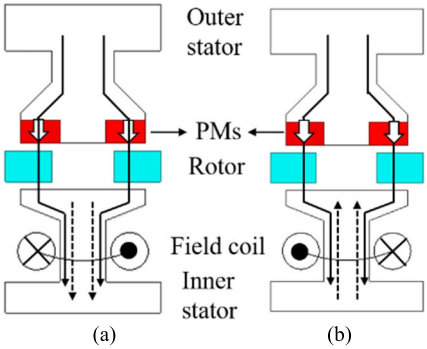

FIGURE 2. Flux path of the DS-HE-FRPM machine. (a) Positive DC field (flux-enhancing). (b) Negative DC field (flux-weakening).

The armature windings are distributed both on the outer and inner stators and have the same winding pattern. A radially magnetized permanent magnet serves as the primary excitation source, generating a constant magnetic field with alternating polarities on adjacent teeth. The DC windings are wound alternately on the inner stator teeth, and produce flux that interacts with the iron poles, enabling flux-enhancing or flux-weakening operation and thereby offering enhanced flexibility in regulating flux-linkage, making it a crucial feature for numerous applications. Halbach PM arrays are positioned on the outer stator teeth, comprising tangentially magnetized PMs placed adjacent to the slot openings. Despite maintaining the same volume of PMs and the structural simplicity as the benchmark design, this Halbach topology aims to reduce leakage flux, improve magnet utilization, and minimize cogging torque of the machine.

In order to further elaborate the working principle of the proposed DS-HE-FRPM machine in this paper, the flux paths during positive and negative excitation currents are illustrated in Figure 2. When a positive DC field is applied, the resulting flux aligns with the primary flux generated by the PMs as depicted in Figure 2(a) and increases the effective flux linkage. Conversely, when a negative DC current is introduced, the flux opposes the primary flux direction as depicted in Figure 2(b) resulting in a lower flux linkage, thereby yielding a weakening effect.

The flux circulation excited by PM under no-load were investigated at various positions of the rotor, and are depicted in Fig. 3. The main circulation path of flux, as indicated by the arrow line, divides into clockwise and counterclockwise directions with varying rotor positions. This division leads to the formation of two poles with opposite polarities. The figures also reveal an alignment of the magnetic field within the designated main flux path in both the inner and outer stators of the DS-HE-FRPM machine, thereby achieving superior magnetic field utilization. Moreover, it demonstrates consistently low leakage flux throughout the structure. These findings demonstrate potential to achieve higher performance capabilities of the structure compared to current state of the art DS- FRPM machines.

The characteristics of the machine under field excitation is examined through the waveforms and spectral analysis of the

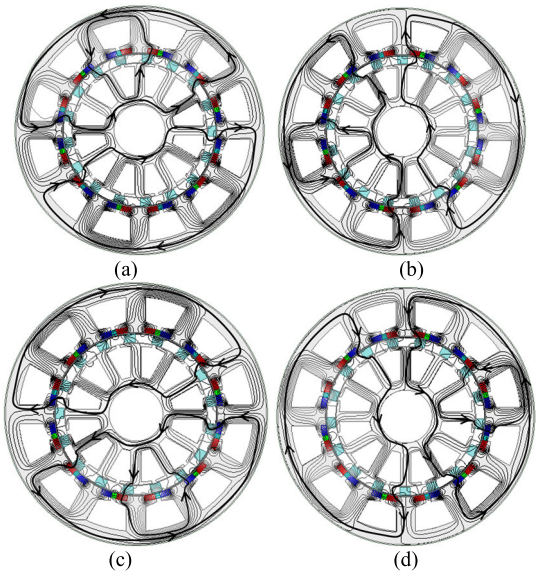

FIGURE 3. No-load flux distribution excited by only PMs at rotor position of (a) 0 (b) 90 (c)180, and (d) 270 electrical degrees.

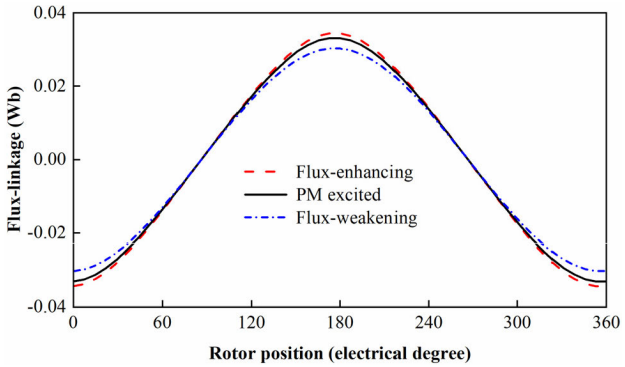

FIGURE 4. No-load phase flux-linkage waveforms under different excitation conditions ($J_{dc} = 4.3$ A/mm^2).

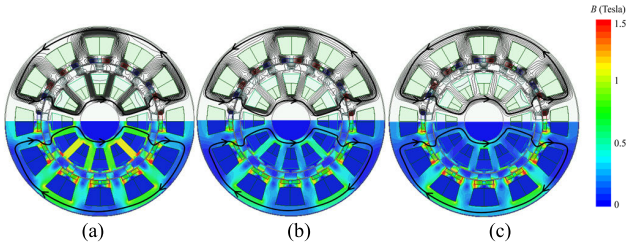

FIGURE 5. Open circuit flux line distribution under different field excitation conditions. (a) $J_{dc} = -4.3$ A/mm^2. (b) $J_{dc} = 0$ A/mm^2. (c) $J_{dc} = 4.3$ A/mm^2.

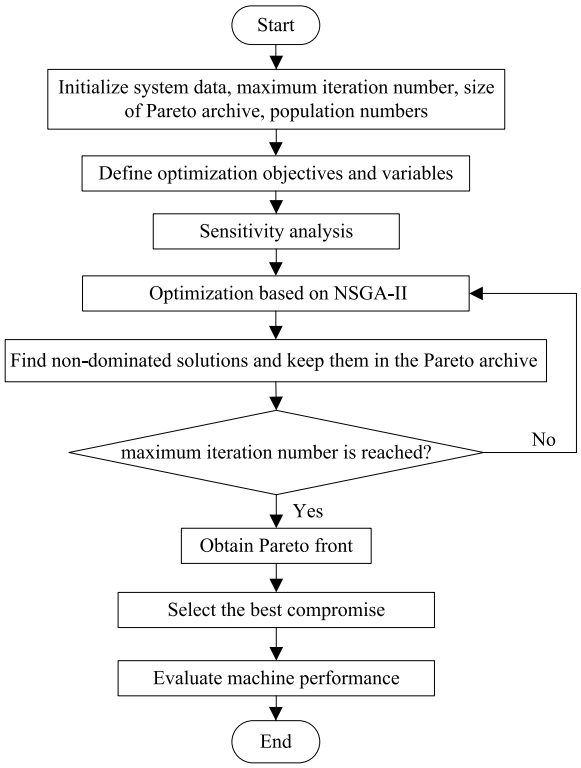

FIGURE 6. Flowchart of the optimization design.

no-load flux linkage under different polarities of a rated DC field current density, J_{dc}, (4.3 A/mm^2), as presented in Fig. 4. At 0° rotor electrical position, both the negative and positive peaks of flux linkage are observed, while the flux linkage reaches zero values at 90° and 270° rotor electrical positions. These characteristics of the flux linkage amplitude variation serve to validate the processes of flux enhancement and weak flux weakening. It is important to note that the waveform of the flux linkage with sole PM excitation aligns well with the flux lines depicted in Fig. 3. Also, a slight change in the flux-linkage under DC field excitations is observed under DC field excitation. The condition of maximum flux linkage is achieved under flux enhancement. The open-circuit flux line distribution of the proposed machine is shown in Fig. 5 under various field excitation conditions. The arrow lines indicate the main flux path. It is evident that the magnetic flux produced by the DC excitation can be overlaid onto the main flux generated by the PMs, leading to a modification in the magnetic flux linkage. Consequently, the magnetic flux density can be regulated in accordance with both the flux-enhancing and flux-weakening conditions.

III. DESIGN OPTIMIZATION USING NSGA-II ALGORITHM

In order to achieve the highest performance of the DS-HE-FRPM, its structural design variables based on their design sensitivity are optimized. The optimization is conducted under flux-enhancing condition which generates the highest flux linkage and maximum electromagnetic torque. Fig. 6 outlines the four-step optimization procedure.

Step 1: Define the objective functions.

Step 2: Select key design variables and their optimization constraints based on sensitivity analysis.

Step 3: Perform the NSGA-II algorithm to optimize the parameters. Obtain the optimal Pareto front.

Step 4: Compare the machine performance before and after optimization.

A. OBJECTIVE FUNCTIONS

The DS-HE-FRPM machine was specifically designed for low-speed high torque traction applications and therefore the primary focus lies on enhancing its torque capability, where

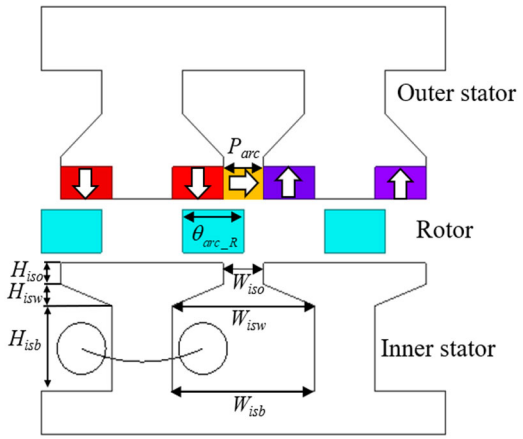

FIGURE 7. Design variables.

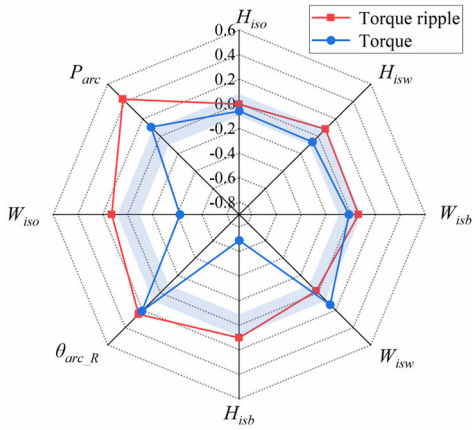

FIGURE 8. Sensitivity of the design variables on the optimization objectives.

the optimization objective functions are defined to attain the goals of maximizing average torque, T_{avg}, and minimizing torque ripple, T_{rip}.

B. DESIGN VARIABLES AND SENSITIVITY ANALYSIS

The optimization process primarily focuses on the design variables of the rotor and inner stator, while the outer stator remains unchanged. To ensure the robustness of the inner stator, the inter-stator teeth and yoke width were set to a minimum value of 4.5 mm. A definition of the seven selected design variables is provided in Fig. 7. To achieve the best optimization performance as well as minimize computational effort, a sensitivity analysis was conducted on these design parameters. The comprehensive sensitivity index, Sc, is set as (2):

$$\begin{cases} S_c(x) = \lambda_1 \dfrac{\Delta T_{\text{rip}}}{\Delta x} + \lambda_2 \dfrac{\Delta T_{\text{avg}}}{\Delta x} \\ \lambda_1 + \lambda_2 = 1 \end{cases} \tag{2}$$

where x represents the design variable, T_{rip} and T_{avg} are the baseline values for torque ripple and average torque, respectively. The variables Δx, ΔT_{rip} and ΔT_{avg} represent the corresponding rate of change for each parameter with respect to the parameter under optimization. The weight coefficients, λ_1 and λ_2, are assigned values of 0.2 and 0.8, respectively. These weights have been chosen in accordance with the typical requirements for EV traction applications, taking into account that the torque ripple of the machine structure is minimized while also being able to prioritize maximization of the average torque production. To achieve high-precision sensitivity analysis and efficiency, the maximum allowable value of Δx is set to 10% and the threshold value for $S_c(x)$ is set to 0.1. Fig. 8 illustrates the sensitivity of the design variables on the optimization objectives. It shows that θ_{arc_R}, H_{isb}, P_{arc}, W_{isw} and W_{iso} exhibit considerable sensitivity to the objectives. These variables were selected for further optimization, taking into account their relatively high level of sensitivity. Table 2 lists the chosen variables for optimization, along with their corresponding sensitivity-based constraints.

TABLE 2. Ranges of design variables.

Parameters (unit)	Minimum value	Maximum value
Rotor pole arc, θ_{arc_R} (degree)	6.93	8.47
Slot body height, H_{isb} (mm)	12.6	15.4
Middle PM arc, P_{arc} (degree)	1.4	1.71
Slot opening width, W_{iso} (mm)	2.8	3.5
Slot wedge width, W_{isw} (mm)	9.9	12.1

C. OPTIMIZATION USING NSGA-II

The optimization process is carried out based on NSGA-II algorithm [17], [18], considering the sensitivity-based constraints. The flowchart of NSGA-II is shown in Fig. 9. The NSGA-II parameters are as follows: population size is 40, the number of generations is 100, the crossover probability is 0.9, and the mutation probability is 0.2. Two-dimensional Pareto front between the average torque and the torque ripple are shown in Fig. 10. The corresponding optimal solution can be extracted from the Pareto front. Further explanation regarding the determination of the best compromise is provided in the next subsection. To reach convergence and obtain the Pareto optimal solution, the random initial population undergoes iterative processes while ensuring that all constraints are satisfied.

D. FINAL VALUES DETERMINATION

Given that any point on the Pareto front represents a set of candidate optimal values within the Pareto solutions, it becomes essential to determine the best compromise. In the context of PM machine design, the selection of the best compromise is commonly guided by the precise requirements of the specific application of the machine, and in this case is for EV traction applications. Hence, the paramount goal of this research revolves around attaining the highest torque capability encompassing both magnitude and ripple. By analyzing the candidate optimal values depicted in Fig. 10, the best compromise is determined using a trade-off evaluation function that takes into account average torque and torque

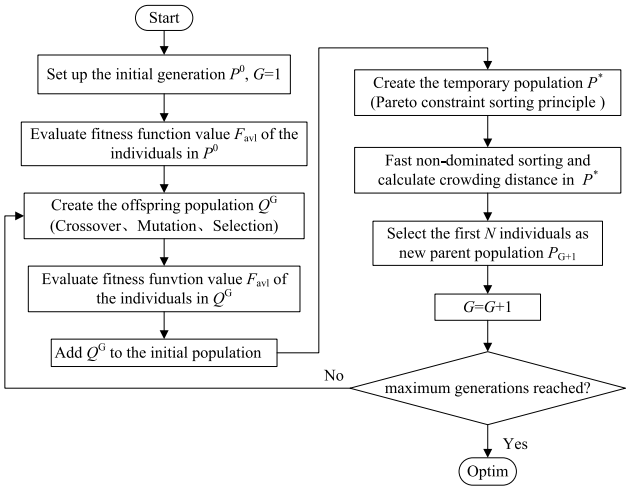

FIGURE 9. The flowchart of NSGA-II.

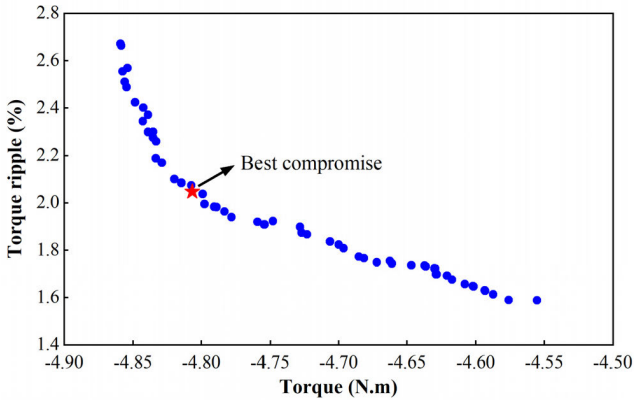

FIGURE 10. Two-dimensional Pareto front of torque and torque ripple at flux enhancing (J_{dc} = 4.3 A/mm^2).

ripple, as outlined in (3) [19]:

$$f_{\text{obj}} = \mu_1 \frac{T'_{\text{avg}}}{T_{\text{avg}}} + \mu_2 \frac{T_{\text{rip}}}{T'_{\text{rip}}} \tag{3}$$

where f_{obj} is the objective function to be minimized, T'_{avg} and T'_{rip} are the initial values of the average torque and torque ripple, respectively. μ_1 and μ_2 are the weight coefficients, where the sum of μ_1 and μ_2 is equal to 1. Based on prior research regarding the optimization design of PM machines, it has been determined that establishing a weight distribution ratio of 8:2 for average torque and torque ripple is deemed suitable for machines intended for EV traction applications. This is particularly relevant in situations demanding high-torque, low-speed performance [20]. Consequently, in this study, μ_1 and μ_2 are assigned values of 0.8 and 0.2, respectively. By utilizing (3) and analyzing the convergence results, the figure demonstrates the identification of the best compromise. A summary of the differences between the average torque, torque ripple, and design variables of the initial and optimal structures is presented in Table 3. The optimized structure displays an average torque of 4.81 N.m, along with a torque ripple of 2.09%. These values indicate improvements

TABLE 3. Parameter of initial and optimal DS-HE-FRPM machines.

Parameters (unit)	Initial value	Optimal value
Rotor pole arc, θ_{arc_R} (degree)	7.7	8
Slot body height, H_{isb} (mm)	14.5	13.5
Middle PM arc, P_{arc} (degree)	1.6	1.55
Slot opening width, W_{iso} (mm)	3.1	3.2
Slot wedge width, W_{isw} (mm)	11	10.5
Output torque, T_{avg} (N.m)	4.39	4.81
Torque ripple, T_{rip} (%)	3.95	2.09

of 9.6% and 47.1%, respectively, when compared to the initial design of the proposed machine.

IV. ELECTROMAGNETIC PERFORMANCE EVALUATION

To validate the DS-HE-FRPM machine and the optimization methodology, the optimized DS-HE-FRPM machine and the benchmark model are compared using 2D finite element analysis. The comparison is conducted at its rated operating speed of 300 r/min, with both machines having identical current densities.

A. BACK-EMF

Fig. 9 displays the waveforms of the back electromotive force (back-EMF) produced due to the PM magnetic fluxes in two machines. In comparison, the DS-HE-FRPM machine exhibits higher peak amplitude of back-EMF, which can be attributed to its higher number of armature winding turns and larger slot area. Additionally, in Fig. 11 (b), it is evident that both machines display a noticeable absence of even harmonics in their back-EMF waveforms. The total harmonic distortion (THD) of the proposed machine is slightly higher than that of the benchmark machine; however, both values remain low and within acceptable limits.

B. COGGING TORQUE

Fig. 12 depicts the cogging torque waveforms of both the DS-HE-FRPM machine and the benchmark. As anticipated, both waveforms display 12 cycles within a single electrical period. Notably, the DS-HE-FRPM machine exhibits a 41.7% lower cogging torque. This significant reduction can be attributed to its more evenly distributed air-gap flux contributed by the wider inner stator tooth tip and Halbach PM arrangement.

C. FLUX REGULATION CAPABILITY

Flux regulation capability plays a vital role in evaluating the electromagnetic performance of hybrid excitation machines [12], [21]. The flux regulation ratio γ, defined by (4) is commonly employed to quantify this effect and is calculated as the ratio between the difference of flux-linkages under flux-enhancing and flux-weakening conditions to the flux-linkage under flux-enhancing [12]:

$$\gamma = (\psi_{\text{enh}} - \psi_{\text{wea}})/\psi_{\text{enh}} \tag{4}$$

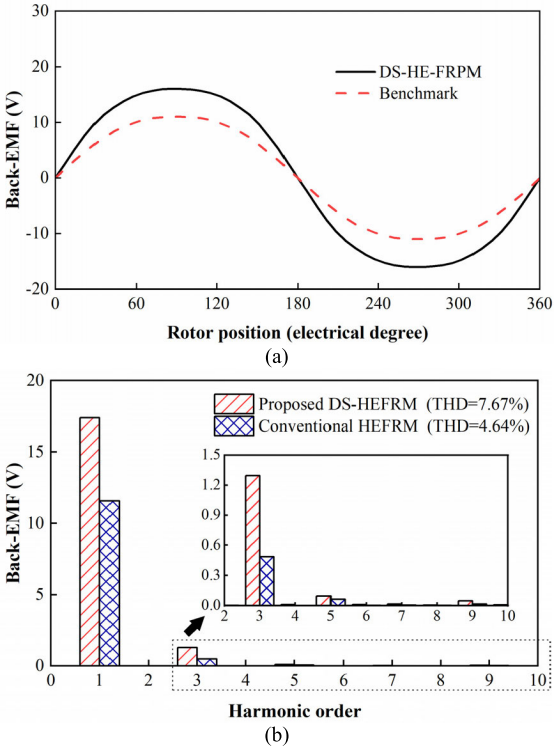

FIGURE 11. Open-circuit phase back-EMF waveforms excited by PMs and its spectra. (a) Waveforms. (b) Harmonics.

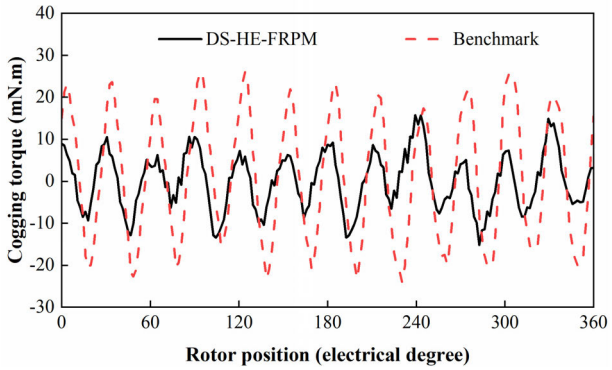

FIGURE 12. Cogging torque waveforms.

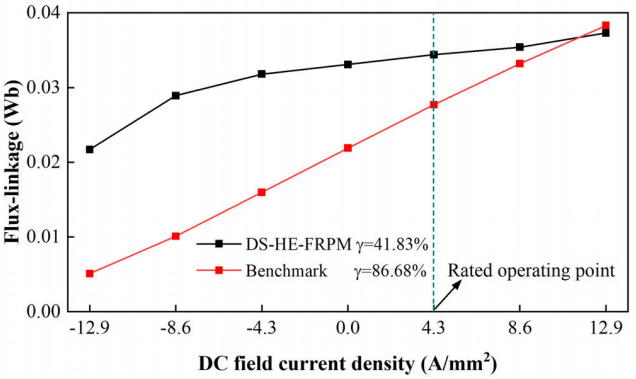

FIGURE 13. No-load flux-linkage under different excitation currents.

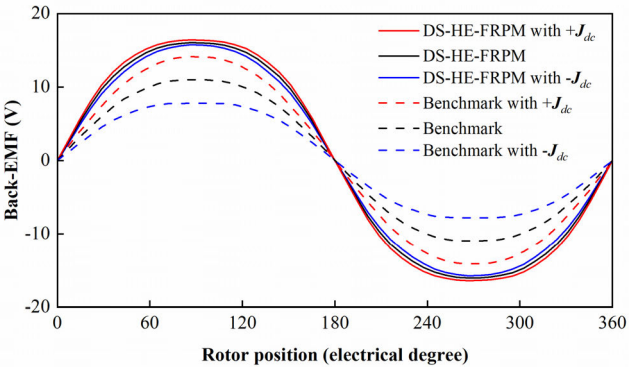

FIGURE 14. Phase back-EMF waveforms under different excitation conditions (J_{dc} = 4.3 A/mm^2).

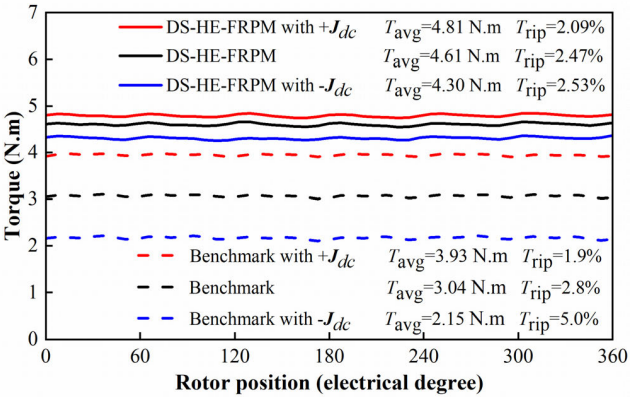

FIGURE 15. Comparison of electromagnetic torque waveforms different excitation conditions (J_{DC} = 4.3 A/mm^2).

where ψ_{enh} and ψ_{wea} represent the flux-linkage under flux-enhancing and flux-weakening conditions, respectively. Fig. 13 provides a comparison of the flux regulation capability between the benchmark and DS-HE-FRPM machine. This assessment is based on their respective no-load flux-linkage and flux regulation ratio at different DC field excitation currents. The DS-HE-FRPM machine exhibits a higher amplitude of flux-linkage but a lower flux regulation ratio. This indicates that while it possesses a strong capability to generate flux, it may face challenges in effectively regulating the flux. Fig. 14 shows the back-EMF waveforms of both machines under different DC excitation conditions. Both machines produce smooth and sinusoidal back-EMF waveforms. Notably, the DS-HE-FRPM machine generates a higher back-EMF than the benchmark in both scenarios. However, it is observed that the benchmark exhibits a wider range of back-EMF variation compared to the DS-HE-FRPM machine.

D. TORQUE AND TORQUE RIPPLE

A comparison of the torque performance between the benchmark and DS-HE-FRPM machine under various field excitation conditions is presented in Fig. 15. When no field excitation current is applied, the DS-HE-FRPM machine exhibits a noteworthy 51.6% improvement in torque with a 11.8% reduction in torque ripple compared to the benchmark. This enhanced torque performance can be attributed to the double-stator topology, which increases the slot area of the armature winding, enabling a higher number of winding

turns. Additionally, Halbach PM arrays improve the utilization of permanent magnets by enhancing the local magnetic field, as well as reduce torque ripple through a more balanced air-gap flux distribution. The torque ripple of the proposed structure remains small and well-maintained under variations in the field excitation current. Furthermore, when the level of field excitation current varies, the DS-HE-FRPM machine demonstrates slight torque variation in contrast to the benchmark model.

To explain this slight variation, consider the following: When the positive DC excitation current is increased, it strengthens the magnetic flux density within the main flux circulation path. This enhancement subsequently leads to a rise in torque. However, if the excitation current exceeds the machine's designated limit, it generates a short-circuit magnetic flux in specific regions. This occurrence, in turn, reduces the distribution of flux along the main flux path. As a result, the torque experiences only a marginal increase at higher DC excitation currents. On the contrary, when a negative DC excitation current is applied to the DS-HE-FRPM machine, it generates a reverse excitation magnetic field that weakens the magnetic field intensity along the main flux path. This condition of flux-weakening consequently leads to a reduction in torque within the proposed structure, owing to the notably stronger flux-weakening capacity compared to the flux-enhancing capacity. The discernible pattern of torque variation aligns harmoniously with the established back-EMF profile intrinsic to the DS-HE-FRPM machine under varying field currents. This observed behavior can be attributed to the relatively restrained capability of the proposed machine to effectively regulate magnetic flux. Alongside this phenomenon, there appears to be a marginal variation in both self and mutual inductances of such a machine across both excitation conditions. Consequently, a prospective avenue to ameliorate these identified constraints involves the augmentation of the DC field intensity. However, it is important to note that this aspect has been deliberately maintained as a design constraint and not considered in this study. Specifically, when considering a rated field excitation current density of 4.3 A/mm^2, the DS-HE-FRPM machine experiences a significantly higher maximum average torque of 4.81 N.m, surpassing the benchmark by 22.4%. Moreover, the analysis reveals that the presence of field excitation has minimal impact on the torque ripple of the DS-HE-FRPM machine, in contrast to the benchmark machine where the torque ripple is greatly influenced by the excitation current. The torque ripple of the optimized DS-HE-FRPM machine is marginally higher than that of the benchmark; nevertheless, it still falls within a range that is both very low and acceptable. In conclusion, the DS-HE-FRPM machine indicates superior electromagnetic performance compared to the benchmark. These results, coupled with the machine's favorable torque characteristics, make it an excellent choice for EV traction applications. In forthcoming efforts, it is recommended to incorporate experimental verification.

V. CONCLUSION

A novel machine, referred to as the DS-HE-FRPM with Halbach PM arrays, was developed for EV traction applications. First, the operating principle of the proposed machine was described, highlighting its superior suitability under flux-enhancing conditions. Subsequently, the sensitivity analysis of structural design variables was conducted before they were optimized using multi-objective optimization based on NSGA-II algorithm to maximize its electromagnetic performance. The proposed machine demonstrated 54.7% higher PM-excited EMF and 41.7% lower cogging torque compared to the benchmark. However, it has slightly worse flux regulation under DC field excitation. The 22.4% improved electromagnetic torque with low ripple of the proposed machine was clearly observed. The reasoning for these enhancements was caused by its double stator topology, reduction of flux leakage, and improved PM utilization rate. Overall, the DS-HE-FRPM machine is a suitable choice for EV traction applications.

REFERENCES

[1] Y. Gao, R. Qu, D. Li, and J. Li, "Torque performance analysis of three-phase flux reversal machines," *IEEE Trans. Ind. Appl.*, vol. 53, no. 3, pp. 2110–2119, May 2017, doi: 10.1109/TIA.2017.2677356.

[2] Y. Gao, D. Li, R. Qu, X. Fan, J. Li, and H. Ding, "A novel hybrid excitation flux reversal machine for electric vehicle propulsion," *IEEE Trans. Veh. Technol.*, vol. 67, no. 1, pp. 171–182, Jan. 2018, doi: 10.1109/TVT.2017.2750206.

[3] C. H. T. Lee, K. T. Chau, C. Liu, T. W. Ching, and M. Chen, "A new magnetless flux-reversal HTS machine for direct-drive application," *IEEE Trans. Appl. Supercond.*, vol. 25, no. 3, pp. 1–5, Jun. 2015, doi: 10.1109/TASC.2015.2388693.

[4] X. Zhu and W. Hua, "An improved configuration for cogging torque reduction in flux-reversal permanent magnet machines," *IEEE Trans. Magn.*, vol. 53, no. 6, pp. 1–4, Jun. 2017, doi: 10.1109/TMAG.2017.2655727.

[5] K. Yang, F. Zhao, Y. Wang, and Z. Bao, "Consequent-pole flux reversal permanent magnet machine with Halbach array magnets in rotor slot," *IEEE Trans. Magn.*, vol. 57, no. 2, pp. 1–5, Feb. 2021, doi: 10.1109/TMAG.2020.3007861.

[6] Y. Meng, S. Fang, Z. Pan, W. Liu, and L. Qin, "Design and analysis of a new partitioned stator hybrid-excited flux reversal machine with dual-PM," *IEEE Trans. Magn.*, vol. 58, no. 2, pp. 1–6, Feb. 2022.

[7] Z. Q. Zhu and S. Cai, "Hybrid excited permanent magnet machines for electric and hybrid electric vehicles," *CES Trans. Electr. Mach. Syst.*, vol. 3, no. 3, pp. 233–247, Sep. 2019, doi: 10.30941/CES-TEMS.2019.00032.

[8] Z. Pan, S. Fang, H. Lin, H. Yang, L. Qin, and S. Lyu, "A new hybrid-excited flux reversal arc permanent magnet machine having partitioned stators for large telescope application," *IEEE Trans. Magn.*, vol. 55, no. 7, pp. 1–10, Jul. 2019, doi: 10.1109/TMAG.2019.2915137.

[9] F. Wei, Z. Q. Zhu, X. Sun, L. Yan, and J. Qi, "Investigation of asymmetric consequent-pole hybrid excited flux reversal machines," *IEEE Trans. Ind. Appl.*, vol. 58, no. 3, pp. 3434–3446, May 2022, doi: 10.1109/TIA.2022.3151316.

[10] T. Heoung Kim, "A study on the design of an inset-permanent-magnet-type flux-reversal machine," *IEEE Trans. Magn.*, vol. 45, no. 6, pp. 2859–2862, Jun. 2009, doi: 10.1109/TMAG.2009.2018776.

[11] Y. Shen, Q. Lu, and Y. Li, "Design criterion and analysis of hybrid-excited Vernier reluctance linear machine with slot Halbach PM arrays," *IEEE Trans. Ind. Electron.*, vol. 70, no. 5, pp. 5074–5084, May 2023, doi: 10.1109/TIE.2022.3183278.

[12] Y. Du, J. Zhao, F. Xiao, X. Zhu, L. Quan, and F. Li, "Partitioned stator hybrid excitation doubly salient machine with slot Halbach PM arrays," *IEEE Trans. Veh. Technol.*, vol. 70, no. 4, pp. 3187–3196, Apr. 2021, doi: 10.1109/TVT.2021.3065670.

[13] D. Li, R. Qu, and T. A. Lipo, "High-power-factor Vernier permanent-magnet machines," *IEEE Trans. Ind. Appl.*, vol. 50, no. 6, pp. 3664–3674, Nov. 2014, doi: 10.1109/TIA.2014.2315443.
[14] B. Ullah, F. Khan, A. H. Milyani, N. Ahmad, and K. M. Cheema, "Design and analysis of dual-stator hybrid excited linear flux switching machine for long-stroke applications," *IET Electric Power Appl.*, vol. 15, no. 12, pp. 1678–1691, Dec. 2021, doi: 10.1049/elp2.12130.
[15] Y. Gao, R. Qu, D. Li, H. Fang, J. Li, and W. Kong, "A novel dual-stator Vernier permanent magnet machine," *IEEE Trans. Magn.*, vol. 53, no. 11, pp. 1–5, Nov. 2017, doi: 10.1109/TMAG.2017.2698004.
[16] G. Zhao and W. Hua, "Comparative study between a novel multi-tooth and a V-shaped flux-switching permanent magnet machines," *IEEE Trans. Magn.*, vol. 55, no. 7, pp. 1–8, Jul. 2019, doi: 10.1109/TMAG.2019.2900749.
[17] K. Deb, A. Pratap, S. Agarwal, and T. Meyarivan, "A fast and elitist multiobjective genetic algorithm: NSGA-II," *IEEE Trans. Evol. Comput.*, vol. 6, no. 2, pp. 182–197, Apr. 2002, doi: 10.1109/4235.996017.
[18] Y. Hua, H. Zhu, M. Gao, and Z. Ji, "Multiobjective optimization design of permanent magnet assisted bearingless synchronous reluctance motor using NSGA-?" *IEEE Trans. Ind. Electron.*, vol. 68, no. 11, pp. 10477–10487, Nov. 2021, doi: 10.1109/TIE.2020.3037873.
[19] Y. Chen, J. Zhuang, Y. Ding, and X. Li, "Optimal design and performance analysis of double stator multi-excitation flux-switching machine," *IEEE Trans. Appl. Supercond.*, vol. 29, no. 2, pp. 1–5, Mar. 2019, doi: 10.1109/TASC.2019.2891899.
[20] H. Li and Z. Q. Zhu, "Influence of adjacent teeth magnet polarities on the performance of flux reversal permanent magnet machine," *IEEE Trans. Ind. Appl.*, vol. 55, no. 1, pp. 354–365, Jan. 2019, doi: 10.1109/TIA.2018.2867818.
[21] Q. Wang, X. Zhao, and S. Niu, "Flux-modulated permanent magnet machines: Challenges and opportunities," *World Electric Vehicle J.*, vol. 12, no. 1, p. 13, Jan. 2021, doi: 10.3390/wevj12010013.

SHICHAO NING received the B.S. degree in electrical engineering from Binzhou University, Binzhou, China, in 2011, and the M.S. degree in electrical engineering from Liaoning Technical University, Huludao, China, in 2014. He is currently pursuing the Ph.D. degree with the Department of Electrical Engineering, Faculty of Engineering, Khon Kaen University, Thailand. His research interests include optimization and design of permanent magnet machines.

PATTASAD SEANGWONG received the B.S. and M.S. degrees in electrical engineering from Khon Kaen University, Khon Kaen, Thailand, in 2018 and 2020, respectively, where he is currently pursuing the Ph.D. degree with the Department of Electrical Engineering, Faculty of Engineering. His research interests include electrical machines, permanent magnet machines, electric vehicles, electrical motors, electrical generators, and renewable energy.

NUWANTHA FERNANDO (Member, IEEE) received the B.Sc. degree in electrical engineering from the University of Moratuwa, Sri Lanka, in 2008, and the Ph.D. degree from The University of Manchester, U.K., in 2012. He was a Researcher with the University of Nottingham and the University of Oxford. He is currently a Lecturer with the Royal Melbourne Institute of Technology (RMIT), Melbourne. His research interests include electric machines and drives, with a specific emphasis on applications in electric transportation. He is an Editor of the IEEE TRANSACTIONS ON ENERGY CONVERSION.

JONGGRIST JONGUDOMKARN received the B.Eng. and Dipl.-Ing. degrees in electrical engineering and information technology from the Technical University of Munich, Germany, in 2012 and 2013, respectively, and the Ph.D. degree from Osaka University, in 2020. He is currently an Assistant Professor with the Department of Electrical Engineering, Faculty of Engineering, Khon Kaen University, Thailand. His research interests include distributed generators, power quality, electric machine drives, and power conversion.

APIRAT SIRITARATIWAT received the B.Eng. degree in electrical engineering from Khon Kaen University, Thailand, in 1992, and the Ph.D. degree from The University of Manchester, U.K., in 1999. Subsequently, he gained industry experience and worked for a few years. In 1994, he joined the Department of Electrical Engineering, Khon Kaen University, where he is currently associated with the KKU-Seagate Cooperation Research Laboratory, Faculty of Engineering. He has been an active Researcher in the fields of electrostatic discharge, electrical overstress, and electromagnetic interference. He has an impressive record of more than 100 publications in these areas. He is recognized as one of the pioneering researchers in the field of magnetism in Thailand. His significant contributions to this area include extensive work with hard disk drive industries.

PIRAT KHUNKITTI (Member, IEEE) received the B.Eng. (Hons.) and Ph.D. degrees in electrical engineering from Khon Kaen University, Thailand, in 2012 and 2016, respectively. He is currently an Associate Professor with the Department of Electrical Engineering, Faculty of Engineering, Khon Kaen University. His research interests include electrical machines, permanent magnet machines, electric vehicles, electrical motors, electrical generators, and renewable energy. He was a recipient of numerous scholarships from the Thailand Research Fund and the National Research Council of Thailand. He serves as an Editor for the *Asia-Pacific Journal of Science and Technology* and an Assistant Editor for *Engineering and Applied Science Research*.